

Silicon Carbide Coating by Thermal Decomposition of tetramethylsilane

Kyung-Hoon YOON

ABSTRACT

Silicon carbide coating has been studied using a graphite substrate, a mixture of tetramethylsilane and hydrogen or argon at deposition temperature (T) of 950 to 1200°C, total pressure of 20 to 50 torr and carrier gas flow rate of 0 to 90 l/h.

Deposition kinetic study has shown that a transition, from a surface reaction limited process to a diffusion limited one, takes place near 1100°C. Deposition rate depends directly upon the experimental parameters.

The influence of the main process parameters is also discussed to relate the physiochemical properties of the coating to the deposition conditions.

1. Introduction

Silicon carbide (SiC) is one of the leading candidates for high temperature engineering ceramics because of its high hardness, good resistance for oxidation in air and chemical inertness.

Considering the poor sinterability due to its covalent nature, the chemical vapour deposition (CVD) method is one of the most useful techniques for preparing highly pure and dense product at relatively low temperatures.

CVD of SiC is usually performed by thermal decomposition of alkyl groups containing silanes, e.g., monomethyl trichlorosilane (CH_3SiCl_3), dimethyl dichlorosilane ($(\text{CH}_3)_2\text{SiCl}_2$) or trimethyl chlorosilane ($(\text{CH}_3)_3\text{SiCl}$) (tab. 1).

For all experiments, tetramethylsilane (TMS, $(\text{CH}_3)_4\text{Si}$) is used as starting material for the SiC. This material is easy to handle since it is not corrosive and does not readily hydrolyze.

It is expected that silicon carbide can be obtained by a simple pyrolysis of TMS.



This paper deals with the effect of the preparation conditions on the deposition rate and the structural, morphological features of the coating.

Table 1. Precursor of silicon carbide.

Precursor	Fusion point (°C)	Boiling point (°C)
CH ₃ SiCl ₃	- 77,8	66,4
(CH ₃) ₂ SiCl ₂	- 76	70,5
(CH ₃) ₃ SiCl	- 57,7	57,7
CH ₃ SiHCl ₂	- 93	41,5
CH ₃ SiH ₃	-156,5	-57,5
(CH ₃) ₃ SiH	-135,9	6,7
(CH ₃) ₄ Si	-102,2	26,5
(C ₂ H ₅) ₂ SiCl ₂	- 96,5	128
(C ₂ H ₅) ₂ SiH ₂	-134,4	56
(C ₃ H ₇) ₃ SiH		171 - 173

2. Experimental

Silicon carbide coating is prepared by thermal decomposition of tetramethylsilane in hydrogen or argon under various conditions as shown in table 2.

Table 2. The preparation conditions

Parameter	Conditions
Deposition temperature (T)	950 - 1200°C
Total gas pressure (P)	20 - 50 torr
Gas flow rate (D)	
TMS (D _{TMS})	0.3 - 1.2 l/h
H ₂ or Ar	0 - 90 l/h

The substrate (graphite 10mm ϕ x 12mm) placed on the graphite susceptor is heated simultaneously by H.F. induction and by radiant heat from the SiC resistor. SiC resistor insulated by refractory brick is also heated by H.F. induction as illustrated in figure 1.

This configuration is adopted, to simulate the experimental conditions more accurately, required by CVD on the ceramic insulator, for example Si_3N_4 .

Input gas flow rate is regulated with mass flowmeters as TMS is a gas at ambient temperature.

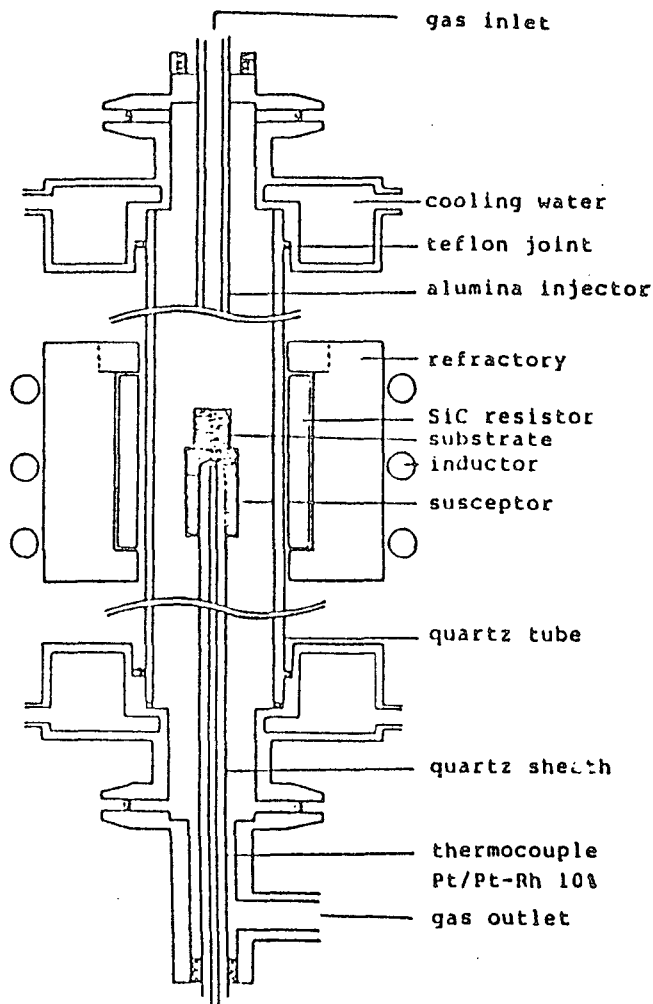


Fig. 1. Deposition chamber

The deposition rate (V) is calculated by measuring the weight increase per unit surface area of the substrate.

The deposits are examined by scanning electron microscopy, X-ray diffractometer and infrared spectrometer. Some coatings are also examined by electron probe microanalyzer to determine the silicon content in the coating.

3. Results and discussion

3.1 Deposition rate

3.1.1 Influence of the temperature

At atmospheric pressure, the deposits are obtained in the form of non-adhesive solid particles for temperatures higher than 1050°C . Experiments are then carried out under the low pressure ($P < 50$ torr).

Fig. 2 represents the time dependence of the weight increase per unit surface area of the substrate (m/s) at 950°C and 1100°C .

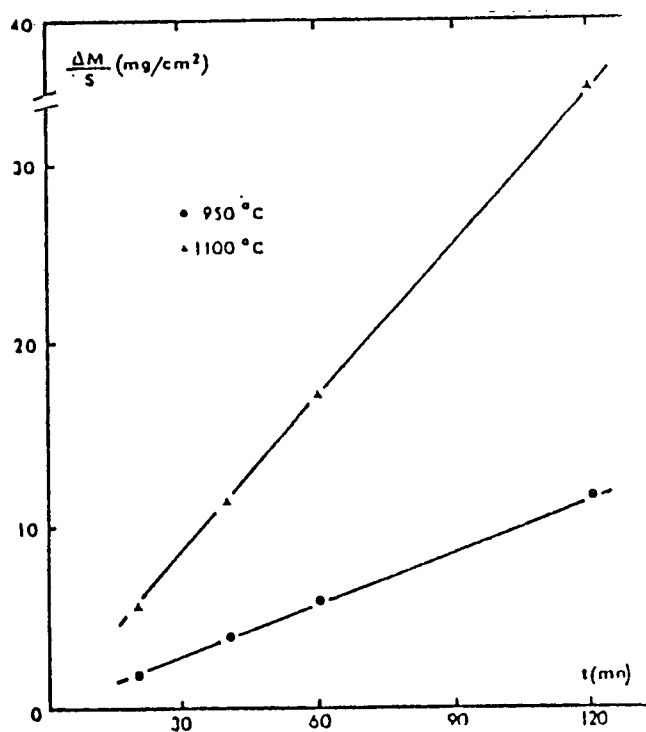


Fig. 2. Time dependence of weight increase ($P=50$ torr, $D_{\text{TMS}} = 0.3$ l/h $D_{\text{H}_2} = 10$ l/h)

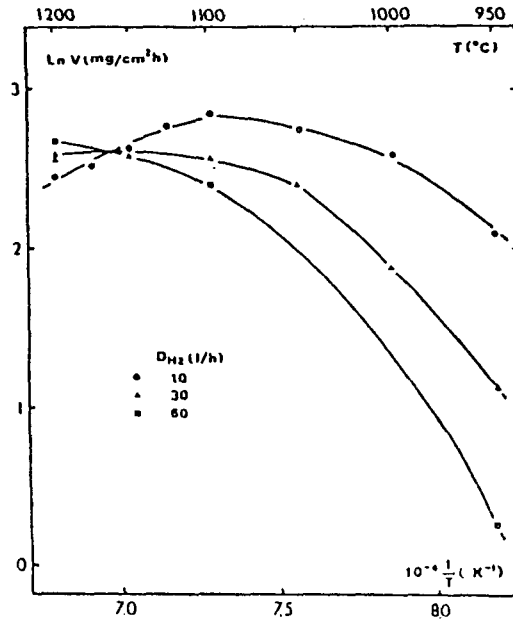


Fig. 3. Arrhenius plot of deposition rate in hydrogen ($P=50$ torr, $D_{\text{TMS}}=0.3$ l/h)

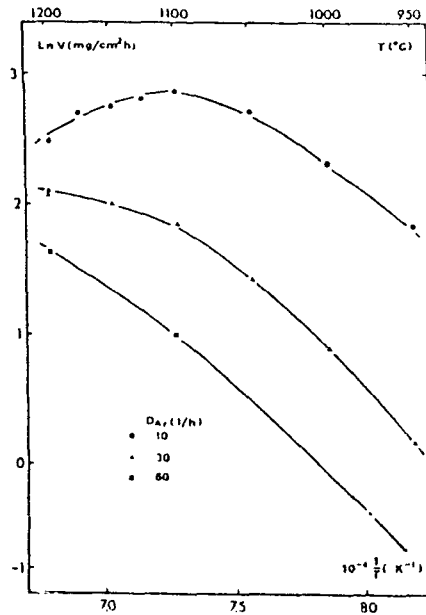


Fig. 4. Arrhenius plot of deposition rate in argon ($P=50$ torr, $D_{\text{TMS}}=0.3$ l/h).

Figs. 3 and 4 show the relations between $\ln V$ and the reciprocal deposition temperature ($1/T$) in the presence of hydrogen and argon, respectively, at 50 torr.

V becomes maximum at about 1100°C at a lower flow rate, while V increases with the temperature up to 1200°C at a higher flow rate.

For a given temperature ($T < 1100^\circ\text{C}$), an increase of carrier gas flow rate leads to a decrease of V .

Using argon as a carrier gas, V is smaller than the case of hydrogen, which is more pronounced at a higher flow rate.

The apparent activation energy observed in the low temperature range ($T < 1100^\circ\text{C}$) tends to increase with the carrier gas flow rate, particularly in the presence of hydrogen.

The temperature of 1100°C can be seen as a transition point between a process limited by surface reactions (low temperature range) and one limited by diffusion of the gaseous species through the boundary layer (high temperature range).

At high temperatures ($T > 1100^\circ\text{C}$) the decrease of V with the temperature at a low flow rate of carrier gas could be related to gas phase reaction which becomes less pronounced or negligible at a higher flow rate of carrier gas.

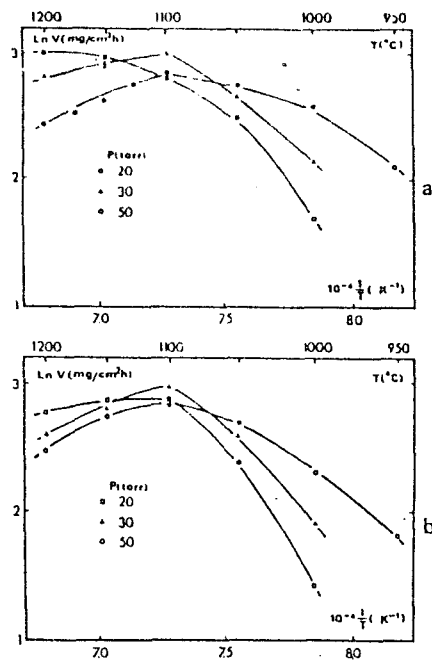


Fig. 5. Arrhenius plot of deposition rate, (a): in H_2 , (b): in Ar ($D_{\text{TMS}}=0.3$ l/h, D_{H_2} , $\text{Ar}=10$ l/h)

3.1.2. Influence of the total pressure

Influence of the total pressure on the deposition rate is studied in the range of 20 - 50 torr for a low flow rate of carrier gas, 10 l/h.

The curves of the Arrhenius plot as shown in figure 5.a,b also indicate the transition near 1100°C as observed before.

In the low temperature range ($T < 1100^\circ\text{C}$), an increase of P is accompanied by an increase of deposition rate. This tendency is reversed at temperatures higher than 1100°C.

At high temperatures, an increase of total pressure induces a decrease in the diffusion coefficient. Moreover, gas phase depletion due to the homogenous reaction is favoured by increasing total pressure.

In the high temperature range where deposition kinetics is controlled by diffusion, diffusive mass transfer is governed by Fick's law, which gives the flux

$$J_i = -D_i/RT \cdot dp_i/dx = D_i/RT \cdot (P_{iv} - P_{is})/\delta$$

where

- D_i ; diffusion coefficient of i
- P_{iv} ; partial pressure of i in the vapour phase
- P_{is} ; partial pressure of i at the interface
- δ ; thickness of the boundary layer

of the i -species as a function of the corresponding partial pressure (P_i) and of the distance (X) to the substrate surface in the boundary layer (2).

It is worth while to mention that in this range, influence of pressure (P) on the deposition rate (V) is much more sensitive to the presence of hydrogen than to argon.

Finally, at 1100°C (the temperature of transition between these two regions), deposition rate shows little dependancy on the total pressure and none on the nature of carrier gas.

3.1.3 Influence of the carrier gas flow rate

The experiments are performed at 950, 1100, 1200°C in the range of 0 to 90 l/h. The total pressure was fixed at 50 torr, the flow rate of TMS at 0.3 l/h.

As shown in figure 6.a,b, at 950°C, V decreases rapidly with the increase of carrier gas flow rate. This is more evident in the presence of argon. At 1100°C, V assumes the maximum value when the flow rate is 10 l/h for hydrogen and 5 l/h for argon. The sharp decrease of V is more pronounced in the case of argon after passing its maximum value.

At 1200°C, for hydrogen, V increases with the flow rate without passing through a maximum. The argon curve remains the same as observed at 1100°C.

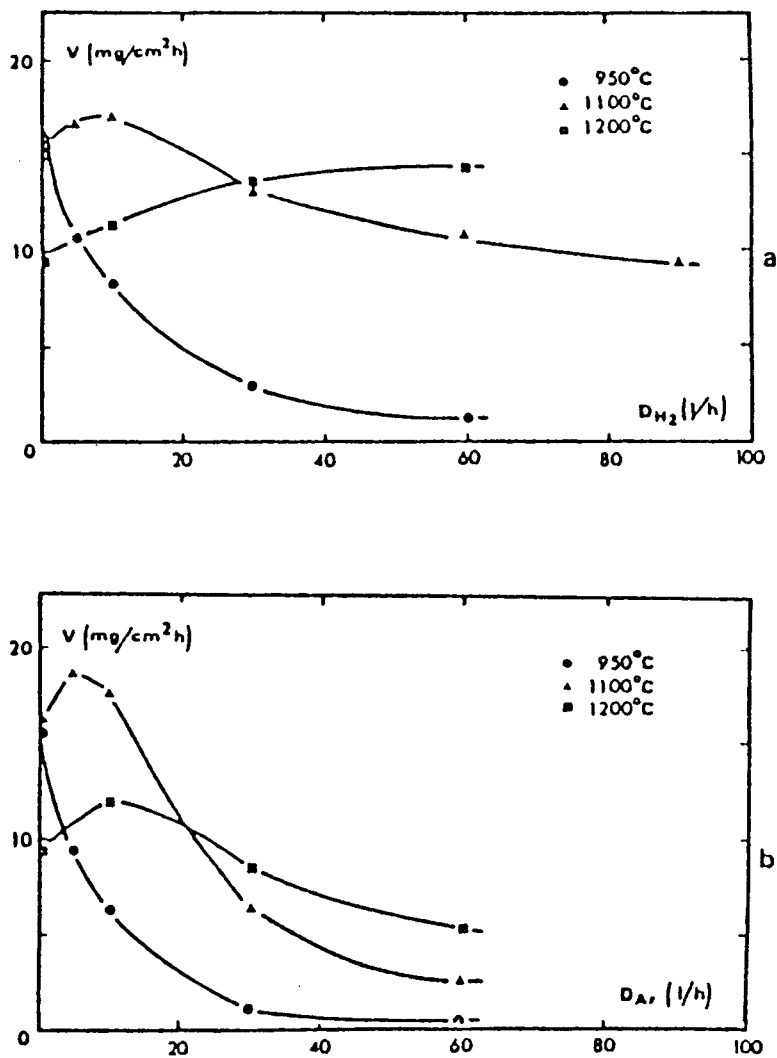


Fig. 6. Variation of the deposition rate as a function of carrier gas flow rate, (a): in H_2 , (b): in Ar ($P=50$ torr, $D_{\text{TMS}}=0.3$ l/h).

In the low temperature range where deposition kinetics is controlled by surface reaction, increasing the carrier gas flow rate induces an increase in the linear velocity of circulating gas above the hot zone of the substrate. In other words, it reduces the residence time of reactive gas. This effect becomes progressively preponderant and results in the decrease of deposition rate, i.e., inversely proportionate to the carrier gas flow rate.

This trend is reversed when the deposition kinetics is controlled by diffusion of reactive species in the boundary layer. Raising the carrier gas flow rate results in an increase of deposition rate by the effect of reduction of boundary layer thickness δ (which vary $D^{-1/2}$) (3). At a higher flow rate, the amount of gaseous reactants consumed by gas phase reaction becomes negligible with respect to that flowing at the gas inlet.

Concerning the influence of nature of carrier gas (H_2 , Ar), the deposition rate is always higher in hydrogen than that in the presence of argon except at high temperatures ($T > 1100^\circ C$) and a low flow rate of 10 l/h.

To take account of the low thermal conductivity of argon compared with that of hydrogen, it can be expected that thermal gradient above the substrate is higher in argon than that in hydrogen. Thermal diffusion effect caused by this phenomenon can hinder the transfer of reactive gas toward the substrate, which consequently promote the gas phase reaction at high temperature.

When the input gas enters the reactor it undergoes an extra acceleration due to the expansion of gas at the hot zone of the reactor. Hotter portions of the gas have higher viscosity and consequently move slower. In order to maintain the constant input gas velocity, the colder parts of the gas stream have to move much faster(4).

In vertical CVD reactors where reactants flow downward through a cylindrical reactor enclosure and impinge upon a heated substrate, a ring of deposited material is often observed on the reactor wall above the susceptor level due to the buoyance effect (5).

Fig. 9 shows the position of solid particles produced by gas phase reaction at $1100^\circ C$ and 50 torr.

When TMS is introduced without using carrier gas, solid particles is located at the upper part of the hot zone as shown in Fig. 7.a. When TMS is introduced with 10 l/h of hydrogen, its position is lowered (Fig.7.b). But introducing the same quantity of argon as a carrier gas, solid particles are distributed uniformly on the lower part of the reactor (Fig. 7.c).

This observation indicates that in the presence of argon, the solid particles caused by gaseous phase reaction runs rapidly through the hot zone of the reactor due to the effect aforementioned. Consequently, using the argon as a carrier gas could hinder the flow of reactants

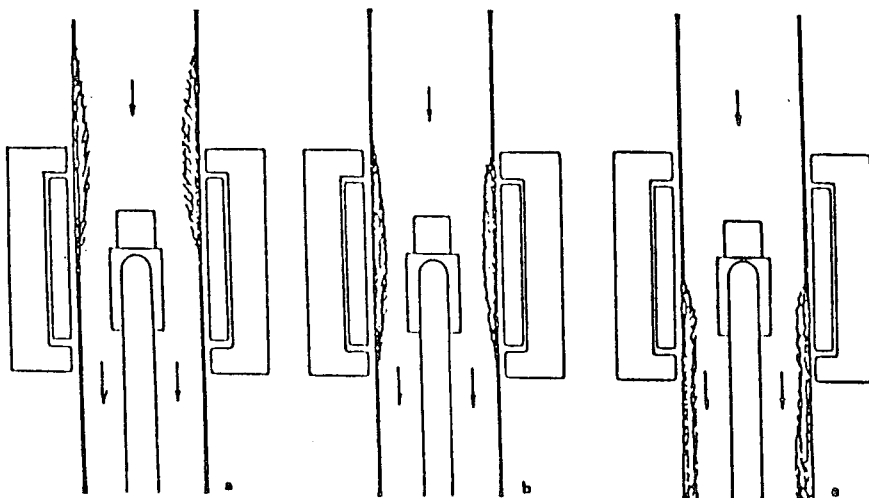


Fig. 7. Localization of the solid particles on the reactor wall, (a): without carrier gas, (b): in H_2 , (c): in Ar, ($T=1100^\circ C$, $P=50$ torr, $D_{TMS}=0.3$ l/h, D_{H_2} , Ar=10 l/h).

toward the substrate by creating a kind of convective turbulent flow pattern.

3.2 Characterization of the coatings

3.2.1 Structure

The X-ray diffraction data show the broadened line corresponding to cubic β -SiC for the coated material deposited above $1050^\circ C$. The presence of graphite is also detected but disappears above $1100^\circ C$. Inclusion of free silicon is not detected by X-ray diffraction.

The infrared transmission spectra of a amorphous deposit show broad band with maxima at approximately 830 cm^{-1} , the characteristics of fundamental vibration of the Si-C bond (Fig. 8).

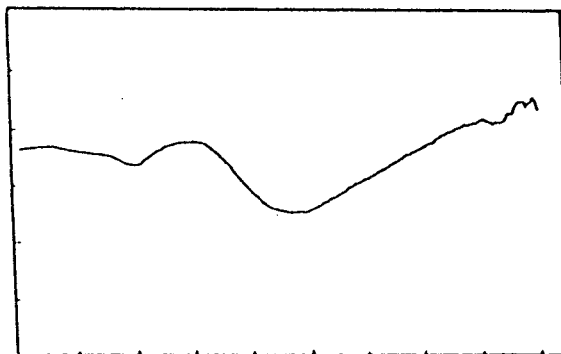


Fig. 8. Infrared transmission spectrum of a coating, ($T=1000^\circ C$)

3.2.2 Morphology

The colour and the morphology of the deposits depend upon the preparation conditions. Up to 1100°C, nodular and fine-grained deposits having bright metallic surface are obtained (Fig. 9.a,b). Above 1100°C the deposits of black matte surface have columnar structure (Fig. 9.c).

At a given temperature, the morphology varies with the nature of carrier gas, its flow rate and the total pressure.

– With respect to the utilisation of pure TMS, H₂ decreases the surface roughness, the lower the total pressure and the temperature the higher the surface smoothness.

– In return, argon is not so effective. Surface smoothness is not ameliorated even at the low pressure and high flow rate. In most cases, deposits obtained in argon atmosphere show a cauliflower feature which appears to be composed of smaller clusters of particles (Fig.9.d).

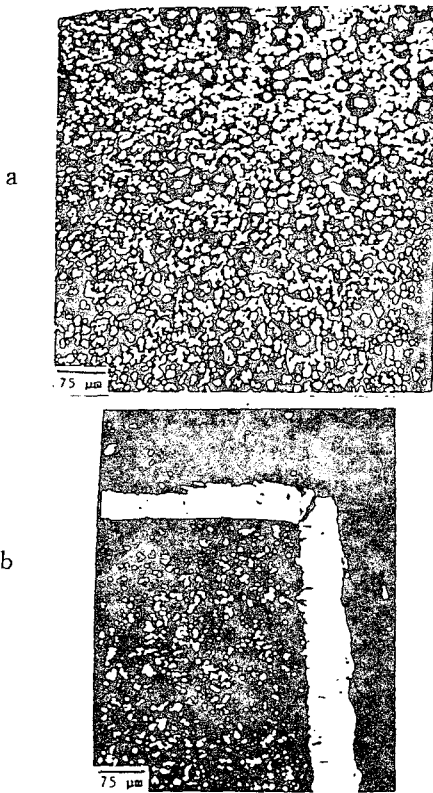


Fig. 9. Morphology of the deposits
 c; T=1200°C, P=30 torr, D_{H₂} =10 l/h
 d; T=1200°C, P=20 torr, D_{Ar} =10 l/h.

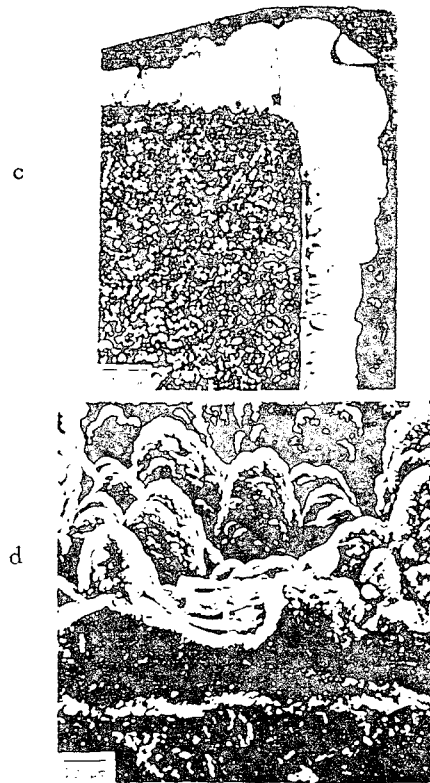


Fig. 9. Morphology of the deposits a,b; T=950°C,
 P=50 torr D_{H₂} =10 l/h.

3.2.3 Chemical composition

The deposited layers produced at 50 torr and carrier gas flow rate of 10 l/h are analyzed by EPMA (Fig. 10).

All the deposits include the free carbon (3-15%) except that obtained in argon at 1150°C.

Between 950°C and 1100°C, free carbon content decreases when the deposits are obtained in hydrogen, while it increases in argon. In both cases, an important discontinuity is observed above 1100°C, temperature that corresponds to the transition of the deposition kinetics, the morphology and the cristallinity of the deposits.

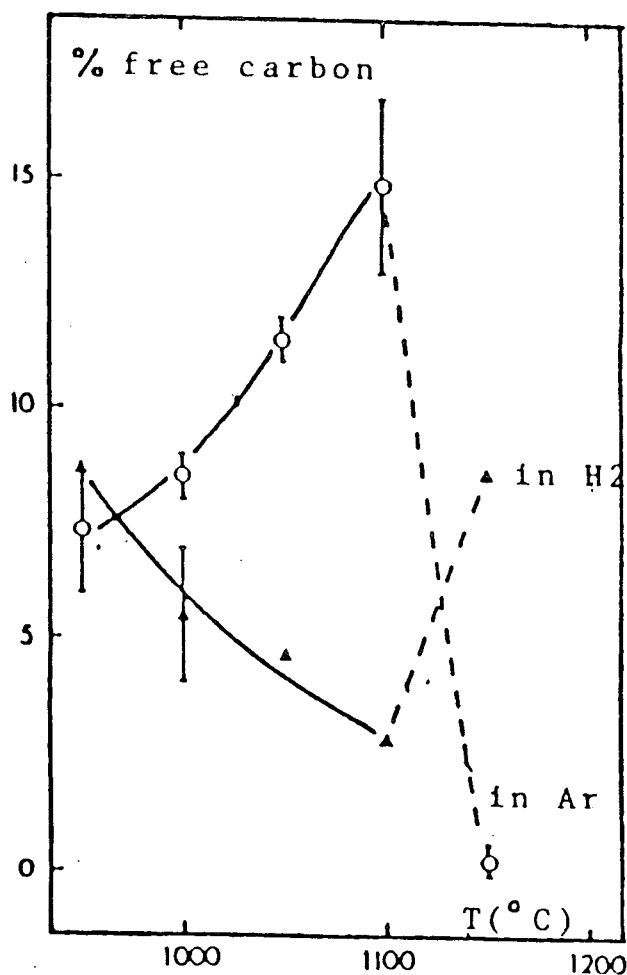


Fig. 10. Free carbon content of the deposits as a function of deposition temperature, ($P=50$ torr, $D_{TMS}=0.3$ l/h, D_{H_2} , Ar=10 l/h).

3.2.4 Crack formation in the deposits

It is observed, both by optical microscopy and S.E.M, that all the deposits are cracked. These cracks could only be seen under the microscope, which forms a network throughout the coating (Fig.11.a). The amount of cracking decreases with an increase of the deposition temperature. This shows little dependency on the total pressure nor the nature of the carrier gas. However, at low temperatures, its formation is favoured by increasing the flow rate of carrier gas (Fig.11.b).

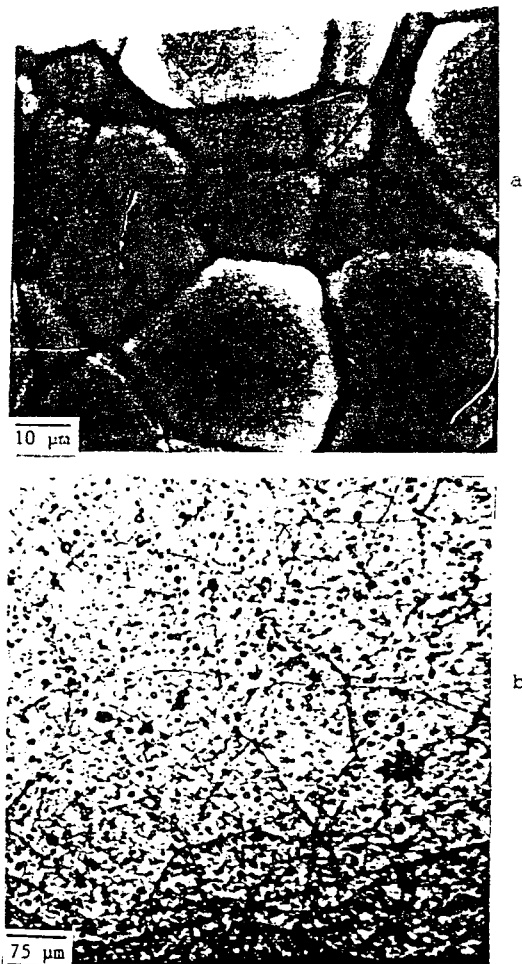


Fig. 11. Microcrack observed in the deposits.
 a; $T=1100^{\circ}\text{C}$, $P=30$ torr, $D_{\text{H}_2}=10$ l/h,
 b; $T=950^{\circ}\text{C}$, $P=50$ torr, $D_{\text{H}_2}=30$ l/h.

Crack formation can be attributed to the existence of microstress or macrostress (6). The major elements causing macrostresses are thermal expansion mismatch and differences in heat conductivity between substrate and coating. The macrostress is generally caused after the deposition due to thermal contraction when the sample is cooled down to the room temperature.

On the other hand, the microstress is usually formed during CVD treatment. Microcracking due to microstress is attributed to microstructural anisotropy in the coating. The conditions which promote the developing (or propagation) of microcracks are as follows; local differences in defect structure, polytypism, composition, porosity, texture, grain size, surface roughness etc.

It is estimated from the present experimental results that microstresses caused by the local difference in chemical composition between stoichiometric and nonstoichiometric zone in the coating could be the main source of cracking: the coating include free carbon.

4. Conclusion

1. The deposition kinetics study shows that there is a transition of the deposition process near 1100°C (surface reaction limited process - diffusion limited process) and the gaseous phase reaction plays an important role in the deposition process, particularly, at a high temperature, high pressure and a low flow rate of the carrier gas.

2. Using argon as a carrier gas leads to a decrease of deposition rate compared with that obtained in hydrogen.

3. Deposits obtained at temperature higher than 1050°C are crystallized.

4. Surface smoothness is ameliorated under the conditions of low temperature, low pressure and high flow rate of carrier gas. From this point of view, the use of argon is not recommended.

5. All the coatings are cracked, but the extent of cracking diminishes with increasing deposition temperature. The principal cause of cracking probably stems from the local difference in chemical composition.

References

1. J. Schlichting, Powder Metall. Int., 12 (1980) 141, 196.
2. C.H.J. van den Brekel, Philips Res. Repts., Part 1, 32 (1977) 118.
3. H. Schlichting, "Boundary Layer Theory", McGraw-Hill, New York, 1968.

4. L.J. Giling, J. Electrochem. Soc., 129 (1982) 634.
5. C. Houtman, H. Moffat and K.F. Jensen, Proc. Euro CVD 5th (1985) p73.
6. P.P.J. Ramaekers and L.R.Wolff, *ibid*, p498.